
# Increasing the Thermoelectric Power Factor of a Semiconducting Polymer by Doping from the Vapor Phase

ACS Macro Letters

Letter

pubs.acs.org/macroletters

# Increasing the Thermoelectric Power Factor of a Semiconducting Polymer by Doping from the Vapor Phase

Shrayesh N. Patel,[†] Anne M. Glaudell,[†,‡] David Kiefer,[†,§] and Michael L. Chabinyc*[,†,‡]

[†]Materials Research Laboratory and [‡]Materials Department, University of California, Santa Barbara, Santa Barbara, California 93106, United States

[§]Department of Chemistry and Chemical Engineering, Chalmers University of Technology, SE-412 96 Gothenburg, Sweden

Supporting Information

**ABSTRACT:** We demonstrate how processing methods affect the thermoelectric properties of thin films of a high mobility semiconducting polymer, PBTTT. Two doping methods were compared: vapor deposition of (tridecafluoro-1,1,2,2-tetrahydrooctyl)trichlorosilane (FTS) or immersion in a solvent containing 4-ethylbenzenesulfonic acid (EBSA). Thermally annealed, thin films doped by FTS deposited from vapor yield a high Seebeck coefficient ($\alpha$) at high electronic conductivity ($\sigma$) and, in turn, a large power factor (PF = $\alpha^2\sigma$) of ~100 $\mu$W m$^{-1}$ K$^{-2}$. The FTS-doped films yield $\alpha$ values that are a factor of 2 higher than the EBSA-doped films at comparable high value of $\sigma$. A detailed analysis of X-ray scattering experiments indicates that perturbations in the local structure from either dopant are not significant enough to account for the difference in $\alpha$. Therefore, we postulate that an increase in $\alpha$ arises from the entropic vibrational component of $\alpha$ or changes in scattering of carriers in disordered regions in the film.

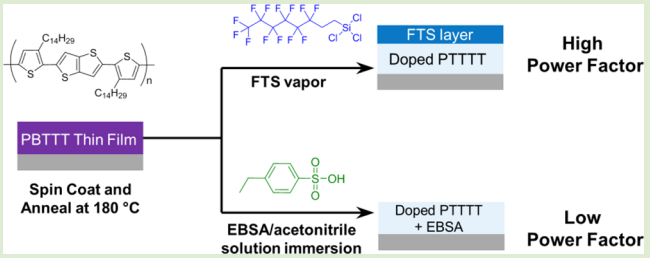




The ability to capture the abundant low-temperature waste heat (<200 °C) using thermoelectric devices can have a profound impact on thermal energy harvesting and management.[1] While inorganic materials have dominated the field,[2] organic semiconductors are candidates for low-temperature applications due to their solution processability and mechanical flexibility, which can enable conformal modules.[3,4] While there are many highly conductive organic materials, the current best *p*-type organic thermoelectrics are based on poly(ethylenedioxythiophene) (PEDOT). It is therefore of great interest to understand if this result is unique or if other materials can be optimized to the level of performance of PEDOT (or greater).

The concentration of charge carriers ($n$) strongly governs the essential properties for thermoelectrics: electronic conductivity ($\sigma$), Seebeck coefficient ($\alpha$), and thermal conductivity ($\kappa$). The thermal to electrical energy conversion efficiency is related to the dimensionless figure of merit, $ZT = \alpha^2\sigma T/\kappa$, where $T$ is the temperature in Kelvin and $\alpha^2\sigma$ is the power factor (PF). Optimizing $ZT$ is quite challenging because each parameter correlates to the carrier concentration of the material—as $n$ increases, $\sigma$ and $\kappa$ increase, and $\alpha$ decreases. In general, $\kappa$ is the sum of both the electronic ($\kappa_e$) and phonon ($\kappa_i$) contributions. Polymers tend to have a low $\kappa_i$, while contributions from $\kappa_e$ may occur at sufficiently high $\sigma$ (~500 S/cm for PEDOT:PSS).[5] Through advances in molecular design and processing techniques, the charge carrier mobilities, $\mu$, of holes and electrons in polymers can now exceed 1 cm$^2$ V$^{-1}$ s$^{-1}$ in field effect devices and should lead to high $\sigma$.[6] The generation of charge carriers in thermoelectric materials, however, is achieved through static electrical doping by molecular species. Therefore, it is of great interest to understand the role of processing in translating the high $\mu$ observed in neat polymers to stably doped systems. Furthermore, it remains an open question what the upper bound for $\alpha$ is at high $\sigma$ for organic materials.[7−9]

Semiconducting polymers can be chemically doped (i.e., by exposure to $I_2$, $NOPF_6$, $F_4TCNQ$, or other oxidants) or electrochemically doped to generate charge carriers.[10−12] In addition to increasing $\sigma$, the introduction of charge carriers affects the magnitude of $\alpha$, which is related to the population in the electronic density of states (DOS) and carrier scattering processes.[13] The introduction of dopants perturbs the molecular packing and likely the morphology relative to the neat material. To achieve electrical conductivities on the order of 100 S/cm, approximately 1/10 monomers would be charged ($n \sim 10^{20}$ cm$^{-3}$) assuming $\mu$ of ~1 cm$^2$ V$^{-1}$ s$^{-1}$. At such high $n$, a strong structural perturbation should likely change the electronic DOS, making it difficult to predict $\alpha$ from models assuming a static DOS (as used in transport studies of thin film transistors). Because of these factors, it is difficult to make predictions of the thermoelectric properties due to the strong coupling with processing methods.

In this letter, we chose to study how processing changes $\sigma$ and $\alpha$ of doped thin films of poly(2,5-bis(3-tetradecylthiophen-

**Received:** December 6, 2015
**Accepted:** January 21, 2016
**Published:** February 5, 2016

  

DOI: 10.1021/acsmacrolett.5b00887
*ACS Macro Lett.* 2016, 5, 268−272

2-yl)thieno[3,2-*b*]thiophene) (PBTTT-$C_{14}$). Specifically, we studied two distinctly different dopants (EBSA, 4-ethylbenzenesulfonic acid, and FTS, (tridecafluoro-1,1,2,2-tetrahydrooctyl)trichlorosilane) (Figure 1). By choosing these

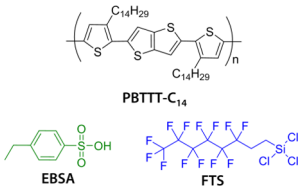


**Figure 1.** Chemical structures for poly(2,5-bis(3-tetradecylthiophen-2-yl)thieno[3,2-*b*]thiophene) (PBTTT-$C_{14}$) and the dopants 4-ethylbenzenesulfonic acid (EBSA) and (tridecafluoro-1,1,2,2-tetrahydrooctyl)trichlorosilane (FTS).

two dopants, we can evaluate how doping from immersion in solvent (EBSA) or from exposure to vapor (FTS) affects the PF at high electrical conductivity (>100 S/cm). Overall, we observe a PF of 110 ± 34 $\mu$W m$^{-1}$ K$^{-2}$ for vapor FTS-doped PBTTT, which is approaching the highest reported PF of 469 $\mu$W m$^{-1}$ K$^{-2}$ for PEDOT:PSS.[14]

PBTTT was chosen because its thin-film microstructure and semiconducting properties have been well-characterized.[15−20] In addition, PBTTT has a liquid crystalline phase that can be used to form highly ordered films by thermal annealing, and thus leading to a high charge-carrier mobility of ∼1 cm$^2$ V$^{-1}$ s$^{-1}$ in thin-film transistors.[21−23] By doping PBTTT-$C_{14}$ after casting and annealing, we can probe how subsequent processing affects the thermoelectric properties. EBSA serves as a small molecule aromatic dopant incorporated from solvent. Thin films are rendered conductive through protonation, and the EBSA anion serves as the counterion for charge neutrality.[24,25] On the other hand, FTS can be deposited from the vapor phase and forms a thin layer on the semiconducting polymer surface.[26] While the precise doping mechanism is still unclear, FTS doping may occur through the following two routes.[26] (1) The FTS layer on the surface of the polymer film induces charge carriers through electrostatic doping arising from the permanent dipole. (2) FTS doping may be occurring through protonic doping from the highly acidic silanol groups present from self-polymerized FTS forming a partially cross-linked siloxane polymer. Because FTS serves as an interfacial dopant, thin films with a thickness around ∼20 nm are needed to render the bulk of the film conductive. In addition, FTS-doped films must be in a $N_2$ atmosphere to ensure long-term stability (∼24 h) as described in more detail in refs 7 and 26. A commonality between EBSA and FTS is the resulting proton-based doping. Detailed doping procedures and atomic force microscopy (AFM) images describing the topography of the doped films can be found in the Supporting Information (Figures S1−S3). In short, PBTTT-$C_{14}$ thin films annealed at 180 °C (18−25 nm) were doped through immersion in an EBSA/acetonitrile solution at varying times. The annealed thin films were FTS doped using a vacuum chamber heated to 80 °C for approximately ∼20 h to reach maximum doping.[26]

UV−vis−NIR optical-absorption measurements reveal that EBSA efficiently dopes PBTTT-$C_{14}$ (Figures S4 and S5). The optical-absorption spectrum of a neat PBTTT-$C_{14}$ has a primary absorption peak at ∼2.20 eV attributed to the $\pi$ to $\pi^*$ transition, which decreases in intensity as a function of increasing doping time. In addition, a new absorption peak develops at ∼1.45 eV along with the development of a broad absorption feature around 0.5 eV at high doping levels corresponding to the combination of polaronic and bipolaronic charge carriers.[27−29] These above transitions do not match the reported charge-modulated absorption spectra for interfacial polarons in PBTTT transistors.[27] The optical absorption of the profile of FTS-doped PBTTT has been reported elsewhere.[26,30]

To evaluate the thermoelectric properties, four-probe in-plane conductivity measurements ($\sigma$) and Seebeck coefficient ($\alpha$) measurements were performed on the doped films. The films were studied as a function of doping time, and the highest-performing $\sigma$, $\alpha$, and PF values are summarized in Table 1. For EBSA doped films, $\sigma$ increases with increasing

**Table 1. Highest-Performing Values for Measured Electrical Conductivity ($\sigma$), Measured Seebeck Coefficient $\alpha$, and Calculated Power Factor (PF)**

| dopant | $\sigma$ (S/cm) | $\alpha$ ($\mu$V/K) | PF ($\mu$W m$^{-1}$ K$^{-2}$) |
|---|---|---|---|
| FTS | 1000 ± 70 | 33 ± 5 | 110 ± 34 |
| EBSA | 1300 ± 10 | 14 ± 2 | 25 ± 7 |

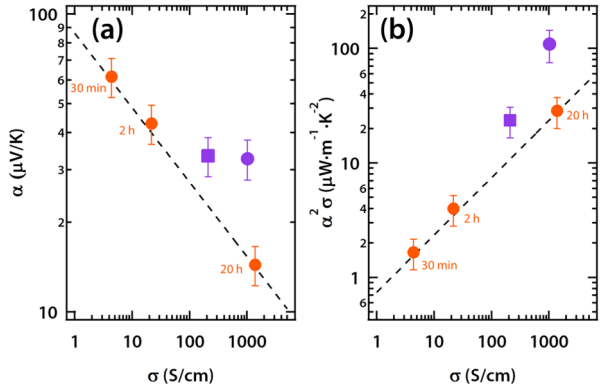


**Figure 2.** (a) Seebeck coefficient ($\alpha$) and (b) power factor (PF = $\alpha^2\sigma$) vs conductivity ($\sigma$) on a log−log scale. Dashed lines are empirical trends [$\alpha = (k_B/e)(\sigma/\sigma_\alpha)^{-1/4}$ and PF = $(k_B/e)^2(\sigma_\alpha\sigma)^{1/2}$] followed by many materials.[7] Orange circles correspond to EBSA-doped films at different immersion times on bare substrate, while purple is for FTS-doped films on bare substrate (circle) and on HMDS-treated substrate (square).

doping time (Figure 2a), while $\alpha$ decreases with doping time. EBSA doping ∼20 h yields $\sigma$ = 1300 S/cm and $\alpha$ = 14 ± 2 $\mu$V/K (PF = 25 ± 7 $\mu$W m$^{-1}$ K$^{-2}$). For the FTS-doped sample, $\sigma$ = 1000 S/cm and $\alpha$ = 33 ± 5 $\mu$V/K (PF = 110 ± 34 $\mu$W m$^{-1}$ K$^{-2}$). The $\sigma$ of FTS-doped PBTTT-$C_{14}$ is in excellent agreement with the work of Kao et al.[26]

Typically, the trends in $\sigma$ and $\alpha$ values are reported as a function of carrier concentration ($n$). However, the quantification of $n$ is quite challenging for chemically doped polymer films due to energetic disorder that makes interpretation of Hall effect measurements difficult.[31] Therefore, we present the trends in $\alpha$ and PF as a function of $\sigma$ (in Figure 2 and Figure S6). It is clear that $\alpha$ is inversely correlated with $\sigma$ for EBSA-doped films—a common correlation between $\alpha$ and $\sigma$. In previous work, an empirical trend for a variety of doped-semiconducting polymers was found where $\alpha$ follows a power law dependence with $\sigma$ ($\alpha \propto \sigma^{-1/4}$) and thus PF follows a


DOI: 10.1021/acsmacrolett.5b00887
ACS Macro Lett. 2016, 5, 268−272

square root dependence with $\sigma$ ($PF \propto \sigma^{1/2}$).[7] The values of $\sigma$ and $\alpha$ follow the empirical trends quite well for EBSA-doped films (Figure 2). Remarkably, the FTS-doped film does not follow the empirical trends, where $\alpha$ and PF are greater than predicted at the high $\sigma$.

The enhancement in $\alpha$ for FTS-doped films may be correlated to the structural properties. Structural perturbations from the physical accommodation of dopant molecules, or from high carrier densities, may strongly perturb the DOS, to which the Seebeck coefficient is directly related. Evaluating how both the EBSA and FTS dopants affect the polymer microstructure is critical in understanding the electrical conductivity and Seebeck coefficient.

We performed grazing incidence wide-angle X-ray scattering (GIWAXS) on the doped films to determine if the two dopants perturbed the local structure differently. 2D GIWAXS images are shown in Figure 3 for pristine, ~20 h EBSA-doped and

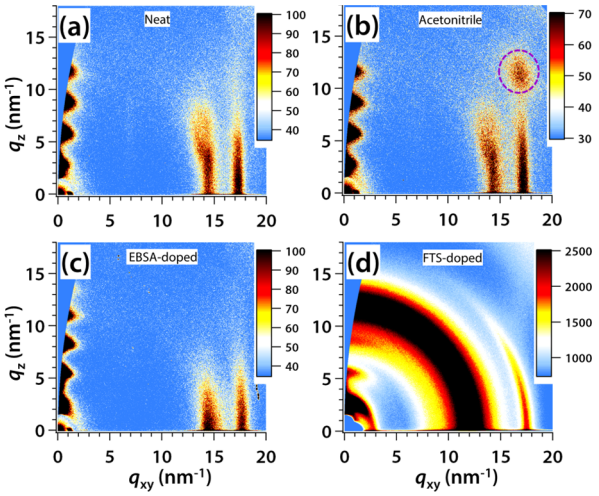


**Figure 3.** GIWAXS images of (a) annealed neat PBTTT, (b) immersed in acetonitrile for ~20 h, (c) EBSA-doped for 20 h, and (d) FTS-doped. The feature (dashed purple circle) in (b) is an artifact arising from scattering from the edges of the substrate.

~20 h FTS-doped PBTTT-$C_{14}$. The intense scattering near the $q_z$ axis corresponds to the lamellar side-chain stacking ($h$00) direction, which indicates the lamella-stacked side chains are oriented out-of-plane (edge-on) relative to the substrate. Along the $q_{xy}$ axis, we observe two scattering peaks at ~14.3 nm$^{-1}$, assigned to the (−11−3) reflection, and at ~17.2 nm$^{-1}$, assigned to (110) and associated with the $\pi$-stacking direction.[18] Comparison between pristine PBTTT-$C_{14}$ and EBSA-doped PBTTT shows a very similar diffraction pattern but with blurring of the off-axis diffraction features. The GIWAXS pattern for a control sample immersed in $CH_3CN$ for ~20 h (Figure 3b) is identical to the pristine PBTTT. This observation highlights that solvent swelling does not account for changes in structural order but entirely from the incorporation of EBSA counterion.

With the FTS-doped film, we observe a strong amorphous halo from $q$ ~ 8 nm$^{-1}$ to ~15 nm$^{-1}$, which corresponds to the scattering from the polymerized FTS layer on the top of the PBTTT film (Figure S7), which obscures some of the scattering features of PBTTT. Nevertheless, we clearly observe the out-of-plane (100) and (200) alkyl stacking reflections and the in-plane $\pi$−$\pi$ stacking reflection. The most obvious difference relative to the pristine pattern is the change in texture that essentially resembles the orientation of an as-cast film. Order parameter calculations indicate that the crystallites still have preferential edge-on orientation (Supporting Information section V). However, it is important to note that crystallite orientation alone does not dictate charge transport in PBTTT but is strongly influenced by the macroscopic charge percolation pathways comprised of crystalline and disordered domains.[16,19,23]

High-resolution specular X-ray scattering on EBSA-doped films reveals the structural perturbations in the alkyl stacking direction ($h$00) (Figure 4, Figure S8 and Table S1). A small

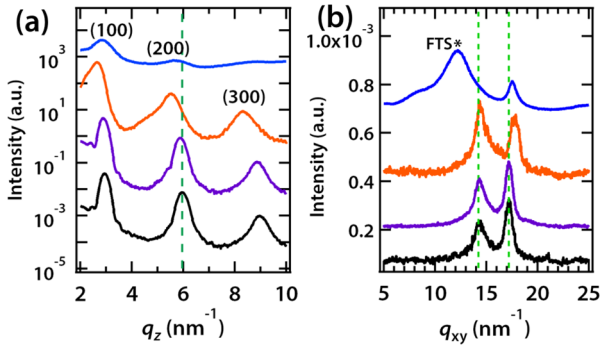


**Figure 4.** (a) High-resolution specular scattering for EBSA-doped films and out-of-plane GIWAXS line cut for FTS-doped film. Vertical dashed green line is a guide for the (200) peak position relative to the pristine film. (b) In-plane ($q_{xy}$) line cuts from GIWAXS for EBSA- and FTS-doped films. The two dashed green lines correspond to the primary peak positions relative to the pristine film. A broad peak at $q_{xy}$ ~ 11 nm$^{-1}$ is from the FTS surface layer. Color scheme: black = neat PBTTT, purple = after immersion in acetonitrile, orange = 20 h EBSA-doped film, and blue = FTS-doped film.

systematic increase in $d$-spacing is observed where $d_{100}$ ~ 2.13 nm for the pristine film and $d_{100}$ ~ 2.36 nm for the ~20 h EBSA-doped film. A film after immersed in just $CH_3CN$ has a $d_{100}$ ~ 2.16 nm, which suggests solvent swelling from $CH_3CN$ has a minimal effect on its own. Thus, the increase in $d$-spacing is primarily from the incorporation of the EBSA anion. For comparison, when PBTTT is blended with PCBM (phenyl-$C_{61}$-butyric acid methyl ester), which is about 1 nm in diameter, $d_{100}$ increases by ~0.9 nm due intercalation into the aliphatic side chains and a change in the tilt of the PBTTT backbone.[32] On the other hand, our EBSA-doped PBTTT only results in an increase in $d_{100}$ by ~0.23 nm, which is significantly smaller than the van der Waals radius of ~1.3 nm of the EBSA anion. The overall similarity of the scattering pattern suggests that EBSA incorporation likely does not strongly change the packing of the PBTTT chains in the crystallites.

The change in peak width in the ($h$00) direction reveals the degree of paracrystalline disorder (Table S1 and Figure S9). Relative to pristine PBTTT, there is an increase in paracrystalline disorder as a function of EBSA doping time. The crystallite size in the lamellar alkyl stacking direction is ~20 nm for pristine PBTTT, ~19 nm after immersion in just $CH_3CN$, and ~13 nm for the ~20 h EBSA-doped film. This is further evidence of increased disorder in the alkyl stacking direction is entirely from the EBSA anion incorporation. High-resolution specular scattering on a FTS-doped film is challenging due to significant background scattering from the FTS surface layer. Therefore, we looked at the out-of-plane scattering from the 2D GIWAXS (Figure 3d, Figure 4a, Figure S11, and Table S3).



DOI: 10.1021/acsmacrolett.5b00887
ACS Macro Lett. 2016, 5, 268−272

While only a minor increase in *d*-spacing occurs only in the alkyl stacking direction ($d_{100}$ = 2.22 nm), a significant increase in peak width indicates that FTS significantly increases disorder in the alkyl stacking direction. However, despite the difference in chemical structure between FTS and EBSA, it is clear that both affect the order and *d*-spacing in the alkyl stacking direction.

Evaluating the perturbation in the $\pi$-stacked regions (a dominant pathway for charge transport[23]) is also critical in understanding the thermoelectric properties. For all the EBSA-doped films studied, the (−1 1−3) reflection does not change significantly as a function of doping time. On the other hand, we do observe a change in the (110) peak position with EBSA doping time (Figure 4b, Figure S10, and Table S2). The *d*-spacing decreases from 0.365 nm for pristine PBTTT to 0.353 nm for ∼20 h EBSA-doped PBTTT. In addition, using the peak width of the (110) reflection, the crystal correlation length (CCL) decreases from 7.20 nm for pristine PBTTT-$C_{14}$ to 5.67 nm for ∼20 h EBSA-doped PBTTT-$C_{14}$. With FTS doping, the *d*-spacing slightly decreases ($d_{110}$ ∼ 0.359 nm) and has a corresponding CCL of 6.20 nm (Figure 4b, Figure S12, and Table S3). Overall, both doping methods bring the conjugated backbones closer together and yield similar CCL values at high doping levels.

The local order of the thin films does not change substantially enough to explain the observed enhancement in Seebeck coefficient of the FTS doping method. If we assume that $\sigma$ for FTS-doped films is enhanced from the value expected from the empirical trend in $\alpha$, it would require the FTS-doped films to have nearly an order of magnitude fewer carriers assuming constant mobility. Such a discrepancy in carrier concentration would likely manifest as a much-reduced transparency for the EBSA-doped films, which is not the case. Alternatively, it is possible that FTS dopes the disordered regions more effectively than EBSA, an effect that would not be revealed by GIWAXS, thereby increasing the number of percolation pathways through additional carriers and leading to an increase in the apparent mobility by ∼10×.

Modifying the polarity of the substrate using a self-assembled monolayer (SAM) can improve the charge carrier mobility of a semiconducting polymer in field-effect transistors. In turn, we FTS-doped a PBTTT-$C_{14}$ thin film on a quartz substrate treated with a HMDS SAM. The value of $\sigma$ was 200 S/cm, and the $\alpha$ value was 34 ± 5 $\mu$V/K. While we do observe a lower $\sigma$ relative to the bare substrate, the $\alpha$ and PF (22 ± 5) values are above the empirical trends. More importantly, $\alpha$ values are equal within error between the FTS-doped samples, providing insight into the mechanism for the enhancement in $\alpha$.

Consequently, we need to examine the different contributions to $\alpha$. Bubnova et al. observed an enhancement in $\alpha$ at high $\sigma$ for a semimetallic PEDOT−Tosylate system where all the charge carriers are bipolarons. For FTS-doped films, electron spin resonance (ESR) measurements[30] and IR spectroscopy measurements[33] indicate a phase separation of metallic and polaron pair domains. As such, FTS-doped PBTTT films do not appear to exhibit semimetallic behavior. Emin presented a general formalism that $\alpha$ for polaronic systems is the sum of the entropy of mixing, spin entropy, and vibrational entropy ($\alpha_{presence}$) and a mechanism-dependent transport entropy ($\alpha_{transport}$).[34,35] It has been observed in boron carbide[36] and pentacene[37] that the vibrational contribution is quite significant, thus enhancing $\alpha$. More recently, field-effect modulated $\alpha$ measurements on various high-mobility semiconducting polymers showed the vibrational contribution can potentially be in the range of 50−100 $\mu$V/K.[38] However, the field-effect modulated measurements are on pristine polymer films, whereas we have doped films with a strong local structural perturbation. Whether the enhancement is due to changes in the vibrational contribution or differences in scattering at domain boundaries is not possible to discern at this point.

The observed PF of 110 ± 34 $\mu$W m$^{-1}$ K$^{-2}$ for our FTS-doped sample is one of the highest reported values for an extrinsically doped polymer film (see Table S4). Our FTS-doped films have a much higher PF relative to other systems extrinsically doped. For example, PBTTT-$C_{14}$ immersion doped with $NOPF_6$ yielded a maximum PF of ∼1 $\mu$W m$^{-1}$ K$^{-2}$, and PBTTT-$C_{12}$ immersion doped with Fe(III) trimide yielded a maximum PF of ∼14 $\mu$W m$^{-1}$ K$^{-2}$ due to a lower Seebeck coefficient than observed here.[39] In contrast, vapor-polymerized PEDOT in the presence of the tosylate anion yielded a high PF value ∼460 $\mu$W m$^{-1}$ K$^{-2}$.[40] With respect to molecular design, one must consider the effect of packing density of the backbone for PEDOT (no side chains) and PBTTT (with long insulating side chains). Endrődi et. al showed that poly(3-alkylthiopene)s with short alkyl side chains yield higher values of PF.[41] If PBTTT can be solubilized with shorter side chains, one would suspect the resulting densely packed structure can result in an additional increase in PF from a higher $\sigma$.

In summary, we find that vapor-doped films of PBTTT-$C_{14}$ yielded better thermoelectric performance (Seebeck coefficient ∼33 $\mu$V/K and power factor ∼100 $\mu$W m$^{-1}$ K$^{-2}$) that exceeded that of solution-doped films formed using comparable processing conditions prior to doping. Extracting ZT is difficult due to the anisotropy expected in thermal transport and the lack of a method to measure the thermal conductivity in the direction of charge transport in these thin organic films. Nevertheless, our results demonstrate that there is not a simple connection between $\alpha$ and $\sigma$ in semiconducting polymers. The differences in the perturbation of the molecular packing between doping methods does not account for the enhancement in $\alpha$ at high $\sigma$. We postulate that the increase in thermoelectric performance may arise from an increased contribution of the disordered regions or from the entropic vibrational contribution to $\alpha$. Our work further reiterates that it is difficult to readily predict thermoelectric properties from the chemical structure of the semiconducting polymers, but the dependence on processing must be considered.

## ■ ASSOCIATED CONTENT

### Supporting Information

The Supporting Information is available free of charge on the ACS Publications website at DOI: 10.1021/acsmacrolett.5b00887.

Experimental methods, AFM images, UV−vis−NIR results, X-ray scattering data, and summary of thermoelectric results (PDF)

## ■ AUTHOR INFORMATION

### Corresponding Author

*E-mail: mchabinyc@engineering.ucsb.edu (M.L.C.).

### Author Contributions

The manuscript was written through contributions of all authors. All authors have given approval to the final version of the manuscript.



DOI: 10.1021/acsmacrolett.5b00887
*ACS Macro Lett.* 2016, 5, 268−272

### Notes

The authors declare no competing financial interest.

## ■ ACKNOWLEDGMENTS

The authors gratefully acknowledge support through the AFOSR MURI program under FA9550−12−1−0002. A.M.G. received partial support from the ConvEne IGERT Program of the National Science Foundation under NSF-DGE 0801627. Use of the Stanford Synchrotron Radiation Lightsource, SLAC National Accelerator Laboratory, is supported by the U.S. Department of Energy, Office of Science, Office of Basic Energy Sciences, under Contract DE-AC02-76SF00515.

## ■ REFERENCES

(1) Johnson, I.; Choate, W. T.; Davidson, A. *Waste Heat Recovery: Technology Opportunities in the US Industry* **2008**, 1−112.
(2) Snyder, G. J.; Toberer, E. S. *Nat. Mater.* **2008**, *7*, 105−114.
(3) Bubnova, O.; Crispin, X. *Energy Environ. Sci.* **2012**, *5*, 9345.
(4) Dubey, N.; Leclerc, M. *J. Polym. Sci., Part B: Polym. Phys.* **2011**, *49*, 467−475.
(5) Liu, J.; Wang, X.; Li, D.; Coates, N. E.; Segalman, R. A.; Cahill, D. G. *Macromolecules* **2015**, *48*, 585−591.
(6) Sirringhaus, H. *Adv. Mater.* **2014**, *26*, 1319−1335.
(7) Glaudell, A. M.; Cochran, J. E.; Patel, S. N.; Chabinyc, M. L. *Adv. Energy Mater.* **2015**, DOI: 10.1002/aenm.201401072.
(8) Kaiser, A. *Phys. Rev. B: Condens. Matter Mater. Phys.* **1989**, *40*, 2806−2813.
(9) Kaiser, A. B. *Rep. Prog. Phys.* **2001**, *64*, 1−49.
(10) Chiang, C. K.; Fincher, C. R.; Park, Y. W.; Heeger, A. J.; Shirakawa, H.; Louis, E. J.; Gau, S. C.; MacDiarmid, A. G. *Phys. Rev. Lett.* **1977**, *39*, 1098−1101.
(11) Yim, K.-H.; Whiting, G. L.; Murphy, C. E.; Halls, J. J. M.; Burroughes, J. H.; Friend, R. H.; Kim, J.-S. *Adv. Mater.* **2008**, *20*, 3319−3324.
(12) Chiang, C. K.; Fincher, C. R.; Park, Y. W.; Heeger, A. J.; Shirakawa, H.; Louis, E. J.; Gau, S. C.; MacDiarmid, A. G. *Phys. Rev. Lett.* **1977**, *39*, 1098−1101.
(13) Fritzsche, H. *Solid State Commun.* **1971**, *9*, 1813−1815.
(14) Kim, G.-H.; Shao, L.; Zhang, K.; Pipe, K. P. *Nat. Mater.* **2013**, *12*, 719−723.
(15) McCulloch, I.; Heeney, M.; Bailey, C.; Genevicius, K.; MacDonald, I.; Shkunov, M.; Sparrowe, D.; Tierney, S.; Wagner, R.; Zhang, W.; Chabinyc, M. L.; Kline, R. J.; McGehee, M. D.; Toney, M. F. *Nat. Mater.* **2006**, *5*, 328−333.
(16) Chabinyc, M. L.; Toney, M. F.; Kline, R. J.; McCulloch, I.; Heeney, M. *J. Am. Chem. Soc.* **2007**, *129*, 3226−3237.
(17) Northrup, J. E. *Phys. Rev. B: Condens. Matter Mater. Phys.* **2007**, *76*, 245202.
(18) Brocorens, P.; Van Vooren, A.; Chabinyc, M. L.; Toney, M. F.; Shkunov, M.; Heeney, M.; McCulloch, I.; Cornil, J.; Lazzaroni, R. *Adv. Mater.* **2009**, *21*, 1193−1198.
(19) Collins, B. A.; Cochran, J. E.; Yan, H.; Gann, E.; Hub, C.; Fink, R.; Wang, C.; Schuettfort, T.; McNeill, C. R.; Chabinyc, M. L.; Ade, H. *Nat. Mater.* **2012**, *11*, 536−543.
(20) Cochran, J. E.; Junk, M. J. N.; Glaudell, A. M.; Miller, P. L.; Cowart, J. S.; Toney, M. F.; Hawker, C. J.; Chmelka, B. F.; Chabinyc, M. L. *Macromolecules* **2014**, *47*, 6836−6846.
(21) DeLongchamp, D. M.; Kline, R. J.; Jung, Y.; Germack, D. S.; Lin, E. K.; Moad, A. J.; Richter, L. J.; Toney, M. F.; Heeney, M.; McCulloch, I. *ACS Nano* **2009**, *3*, 780−787.
(22) Schuettfort, T.; Watts, B.; Thomsen, L.; Lee, M.; Sirringhaus, H.; McNeill, C. R. *ACS Nano* **2012**, *6*, 1849−1864.
(23) Noriega, R.; Rivnay, J.; Vandewal, K.; Koch, F. P. V; Stingelin, N.; Smith, P.; Toney, M. F.; Salleo, A. *Nat. Mater.* **2013**, *12*, 1038−1044.
(24) Nam, S.; Kim, J.; Lee, H.; Kim, H.; Ha, C.-S.; Kim, Y. *ACS Appl. Mater. Interfaces* **2012**, *4*, 1281−1288.
(25) Hosono, K.; Matsubara, I.; Murayama, N.; Shin, W.; Izu, N. *Thin Solid Films* **2005**, *484*, 396−399.
(26) Kao, C. Y.; Lee, B.; Wielunski, L. S.; Heeney, M.; McCulloch, I.; Garfunkel, E.; Feldman, L. C.; Podzorov, V. *Adv. Funct. Mater.* **2009**, *19*, 1906−1911.
(27) Zhao, N.; Noh, Y.-Y.; Chang, J.-F.; Heeney, M.; McCulloch, I.; Sirringhaus, H. *Adv. Mater.* **2009**, *21*, 3759−3763.
(28) Beljonne, D.; Cornil, J.; Sirringhaus, H.; Brown, P. J.; Shkunov, M.; Friend, R. H.; Brédas, J.-L. *Adv. Funct. Mater.* **2001**, *11*, 229−234.
(29) Brown, P. J.; Thomas, D. S.; Köhler, A.; Wilson, J. S.; Kim, J.-S.; Ramsdale, C. M.; Sirringhaus, H.; Friend, R. H. *Phys. Rev. B: Condens. Matter Mater. Phys.* **2003**, *67*, 064203.
(30) Tanaka, H.; Hirate, M.; Watanabe, S.; Kuroda, S. I. *Adv. Mater.* **2014**, *26*, 2376−2383.
(31) Wang, S.; Ha, M.; Manno, M.; Daniel Frisbie, C.; Leighton, C. *Nat. Commun.* **2012**, *3*, 1210.
(32) Miller, N. C.; Cho, E.; Gysel, R.; Risko, C.; Coropceanu, V.; Miller, C. E.; Sweetnam, S.; Sellinger, A.; Heeney, M.; McCulloch, I.; Brédas, J. L.; Toney, M. F.; McGehee, M. D. *Adv. Energy Mater.* **2012**, *2*, 1208−1217.
(33) Khatib, O.; Lee, B.; Yuen, J.; Li, Z. Q.; Di Ventra, M.; Heeger, a. J.; Podzorov, V.; Basov, D. N. *J. Appl. Phys.* **2010**, *107*, 123702.
(34) Emin, D. *Phys. Rev. B: Condens. Matter Mater. Phys.* **1999**, *59*, 6205−6210.
(35) Emin, D. *Phys. Status Solidi B* **1998**, *205*, 385−390.
(36) Aselage, T. L.; Emin, D.; McCready, S. S.; Duncan, R. V. *Phys. Rev. Lett.* **1998**, *81*, 2316−2319.
(37) von Mühlenen, A.; Errien, N.; Schaer, M.; Bussac, M.-N.; Zuppiroli, L. *Phys. Rev. B: Condens. Matter Mater. Phys.* **2007**, *75*, 115338.
(38) Venkateshvaran, D.; Nikolka, M.; Sadhanala, A.; Lemaur, V.; Zelazny, M.; Kepa, M.; Hurhangee, M.; Kronemeijer, A. J.; Pecunia, V.; Nasrallah, I.; Romanov, I.; Broch, K.; McCulloch, I.; Emin, D.; Olivier, Y.; Cornil, J.; Beljonne, D.; Sirringhaus, H. *Nature* **2014**, *515*, 384−388.
(39) Zhang, Q.; Sun, Y.; Xu, W.; Zhu, D. *Macromolecules* **2014**, *47*, 609−615.
(40) Bubnova, O.; Khan, Z. U.; Wang, H.; Braun, S.; Evans, D. R.; Fabretto, M.; Hojati-Talemi, P.; Dagnelund, D.; Arlin, J.-B.; Geerts, Y. H.; Desbief, S.; Breiby, D. W.; Andreasen, J. W.; Lazzaroni, R.; Chen, W. M.; Zozoulenko, I.; Fahlman, M.; Murphy, P. J.; Berggren, M.; Crispin, X. *Nat. Mater.* **2013**, *13*, 190−194.
(41) Endrődi, B.; Mellár, J.; Gingl, Z.; Visy, C.; Janáky, C. *J. Phys. Chem. C* **2015**, *119*, 8472−8479.



DOI: 10.1021/acsmacrolett.5b00887
*ACS Macro Lett.* 2016, 5, 268−272